The Electronic Structure of $[Te_{15}Br_4][MoOBr_4]_2$ and Some General Aspects of Bonding in "Classical" and Hypervalent Tellurium Halides

Gregory A. Landrum, Norman Goldberg, and Roald Hoffmann*

Department of Chemistry and Materials Science Center, Cornell University
Ithaca, New York 14853-1301, U.S.A.

Received October 29, 1996

Keywords: Hypervalent compounds / Tellurium / Polycations / Molecular Orbital Theory / Band structure

Approximate MO and band structure calculations are used to analyze the bonding in the recently synthesized paramagnetic, semi-conducting phase $[Te_{15}Br_4][MoOBr_4]_2$. This compound is made up of 2 types of isolated one-dimensional subchains: $[MoOBr_4]^-$ and $[Te_{15}Br_4]^{2+}$. The $[Te_{15}Br_4]^{2+}$ chains are very similar to those in the tellurium subhalide Te_2Br. The electronic structure and bonding within these chains is analyzed and the possibility of hypervalency in both $[Te_{15}Br_4][MoOBr_4]_2$ and Te_2Br is discussed. The bonding in the classically hypervalent molecule $TeBr_4^{2-}$ and a model $Te_3Br_2^{4-}$ is compared to that of the infinite system. Our calculations indicate that both $[Te_{15}Br_4][MoOBr_4]_2$ and Te_2Br contain weakly hypervalent Te atoms and that the interesting electronic properties of $[Te_{15}Br_4][MoOBr_4]_2$ arise within the distinct sublattices, which do not interact significantly.

Whether in nonclassical hypervalent phases[1–6], or in polycations[7–10], the amazingly rich structural chemistry of tellurium continues to intrigue experimentalists as well as theoreticians[11–13]. In this contribution we examine the bonding in the $[Te_{15}X_4]_n[MOX_4]_{2n}$ (M = Mo, W; X = Cl, Br) phase recently reported by Beck et al.[14]. This compound, which consists of infinite $[MOX_4]^-$ and $[Te_{15}X_4]^{2+}$ chains, has an unusual combination of semiconducting and paramagnetic properties. The analysis leads us naturally to look at the bonding in the structurally related Te subhalides Te_2X[15].

The $[Te_{15}X_4]_n[MOX_4]_{2n}$ Structure

A view of the structure of $[Te_{15}X_4]_n[MOX_4]_{2n}$ looking down the one-dimensional chains that comprise it is shown in Figure 1. As this complex structure is built up of distinct $[MOX_4]^-$ and $[Te_{15}X_4]^{2+}$ sublattices, we will consider each in turn.

Figure 1. A perspective view of the crystal structure of $[Te_{15}X_4]_n[MOX_4]_{2n}$; one $[Te_{15}Br_4]^{2+}$ dimer is highlighted (boxed), as is a $[MOX_4]^-$ chain; the labeling code for the spheres is: light Te, light gray M, dark gray X, black O

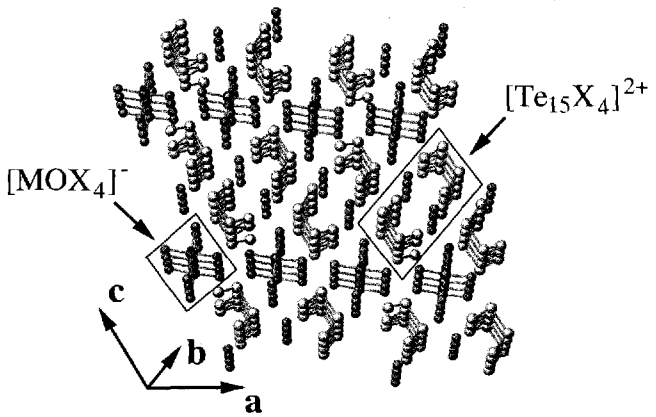

The $[MOX_4]^-$ sublattice is simply described as consisting of one-dimensional chains of vertex-sharing distorted octahedra (**1**). There are two very different M–O distances in this structure, 2.41 and 1.62 Å[16].

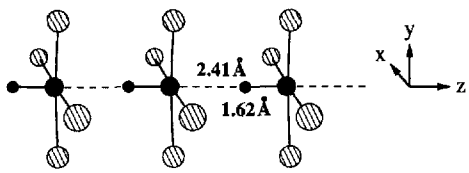

1

The Te chains in the $[Te_{15}X_4]^{2+}$ part of the structure are very similar to those found in the well known Te subhalides (Te_2X)[15]. These subhalides consist of one-dimensional Te chains made up of edge-sharing six-membered rings in a boat conformation, **2**. Notice the twofold bridging halides, pyramidal three-coordinate Te2 and Te3, and roughly square-planar four-coordinate Te1 and Te4.

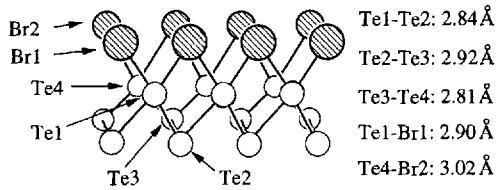

2

In the $[Te_{15}X_4]^{2+}$ sublattice of $[Te_{15}X_4]_n[MOX_4]_{2n}$, similar chains appear in pairs; two such chains are shown in the boxed unit in Figure 1. The major difference between $[Te_{15}X_4]^{2+}$ and the Te subhalides is the presence of "defects"[17]: the X-ray structure indicates that the Te4 site of

  0009–2940/97/0404–0463 $ 17.50+.50/0

$[Te_{15}X_4]^{2+}$ is only 75% occupied. The electronic reasons for the presence of these vacancies will be discussed later.

In our analysis, we focus our attention on one member of the $[Te_{15}X_4]_n[MOX_4]_{2n}$ family: $[Te_{15}Br_4][MoOBr_4]_2$. We examine the electronic structure and properties of $[Te_{15}Br_4][MoOBr_4]_2$ by looking at separated $[Te_{15}Br_4]^{2+}$ and $[MoOBr_4]^-$ subchains; the intent is to provide an explanation for the observed electronic and magnetic properties in this compound. Our computational methodology is the extended Hückel method, an approximate molecular orbital method, which is not good for evaluating energetics, but which gives a reasonable account of the basic electronic structure of quite disparate molecular and extended structures[18–21]. Computational details are given in the Experimental Section.

The Electronic Structure of Te_2Br

Due to the strong structural similarities between Te_2Br and the $[Te_{15}Br_4]^{2+}$ sublattice of $[Te_{15}Br_4][MoOBr_4]_2$, it is instructive to begin with the simpler parent subhalide structure. We build up the structure of Te_2Br by starting with a $[Te_2]^+$ chain (half of the $[Te_4]^{2+}$ backbone), **3**. The band structure, Density of States (DOS), and Te–Te Crystal Orbital Overlap Population (COOP)[18,22] curves for this chain are shown in Figure 2[23].

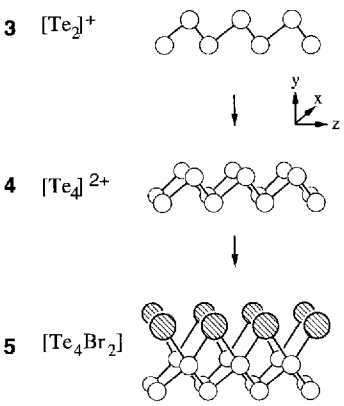

The electronic structure of these $[Te_2]^+$ chains is qualitatively very similar (though the electron count is of course different) to that of the carbon backbone of polyacetylene[24]. In the vicinity of the Fermi level (ε_f) the π bands of the chain (the Te p_x orbitals have π symmetry along the chains in $[Te_2]^+$) and a σ band are found. The latter band has substantial "lone pair" character (along the y direction). This is the band that is reponsible (eventually, when the H's are added to a C_2 chain backbone) for C–H bonding in the polyacetylene structure, and which will be involved in Te–Br interactions when we add the Br^- ions. The Fermi level of the $[Te_2]^+$ chain occurs in the middle of the π^* band.

When two $[Te_2]^+$ chains are brought together to form $[Te_4]^{2+}$, **4**, the orbitals of the π band of each chain interact in a σ manner between chains. However, since the Te2–Te3 and Te1–Te4 distances between chains are very different (Te2–Te3 2.92 Å, Te1–Te4 3.72 Å) this interaction is not at all symmetric. The Te2–Te3 σ and σ^* levels (since the chains are canted with respect to each other, there is no strict σ–π separation; these Te2–Te3 σ bonding levels are derived from the π levels of the building block $[Te_2]^+$ chains) are pushed well away from ε_f, showing up at $\sim$–20 eV and $\sim$–8 eV. However, the much weaker Te1–Te4 interactions leave mainly Te1 and Te4-centered bands in the vicinity of ε_f. In fact, the band directly below ε_f is almost entirely composed of out-of-phase combinations of Te1–Te4 σ orbitals.

The "interaction diagram" for the $[Te_4]^{2+}$ and $[Br_2]^{2-}$ sublattices of $[Te_4Br_2]$ (this is the stoichiometry of the unit cell for Te_2Br used in our calculations), **5**, shown in Figure 4, holds few surprises.

The bands of the $[Br_2]^{2-}$ sublattice are quite flat, since there is little interaction between the bromides due to the 4.00 Å Br–Br distance. In the composite structure, the major contributors to the two bands under ε_f are the Br atoms (Figure 5). These two bands are strongly Te–Br antibonding.

Figure 2. The band structure (left), DOS (center), and Te–Te COOP curves (right) for a $[Te_2]^+$ chain; the horizontal dotted line indicates the position of the Fermi level (ε_f); the dashed line in the COOP figure corresponds to the integration of the COOP curve

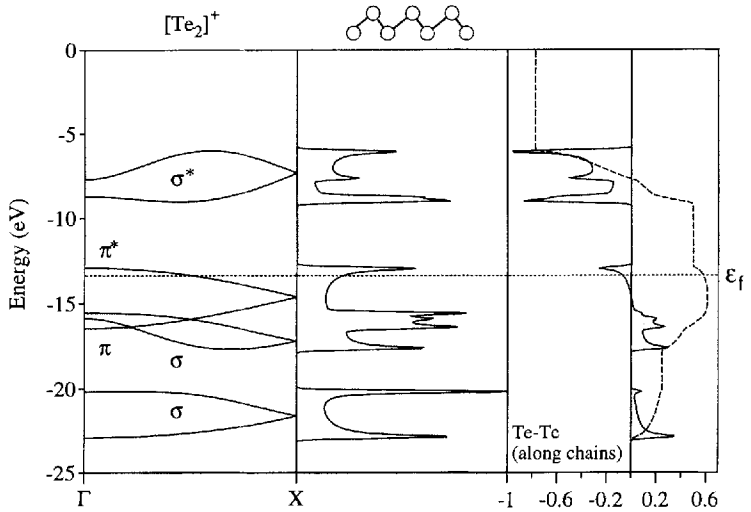

Figure 3. The band structures of $[Te_2]^+$ (left) and $[Te_4]^{2+}$ (right)

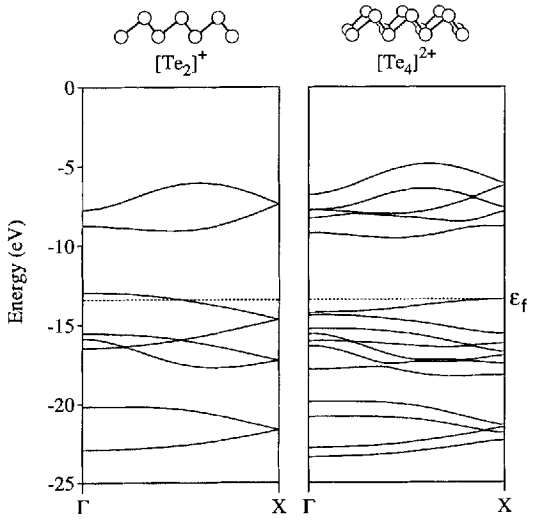

The integrated Te–Br COOP shown in Figure 5 indicates that though the Highest Occupied Crystal Orbitals (HOCOs) are strongly Te–Br antibonding, there are still reasonable Te–Br overlap populations (0.10 between Te1 and Br1 and 0.06 between Te4 and Br2). These overlap populations are, however, smaller than the Te–Br OP in the "classically hypervalent" $TeBr_4^{2-}$[25], 0.19, in keeping with the longer Te–Br bonds (the Te–Br bond length in $TeBr_4^{2-}$ is 2.75 Å, while the lengths in Te_2Br are 2.90 and 3.00 Å). This is a feature of the bonding that we need to understand; a detailed analysis is given below.

The Possibility of Electron-Rich Three-Center or Hypervalent Bonding in Te_2Br

A striking structural feature of Te_2Br is the four-coordinate, roughly square-planar Te center. This is reminiscent of XeF_4, TeX_4^{2-} (X = Cl, Br)[25] and other four-coordinate Te centers in extended structures[1,5]. In these compounds electron-rich three-center (or hypervalent) bonding exists, and it is worthwhile to ask the question whether a similar bonding type occurs in Te_2Br.

The features of electron-rich three-center bonding are well understood for the classical compounds XeF_2 and I_3^-[26–30]. One has in these species three molecular orbitals (see **6** for sketches of these three levels in I_3^-) derived from the interaction of the lone-pairs on the two external atoms with the center atom.

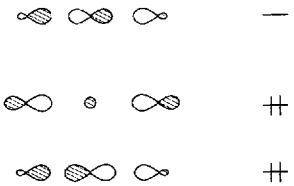

6

The lowest level is strongly bonding, the central is slightly antibonding (mainly due to the mixing in of some s-character on the central atom) and the highest level is strongly antibonding. The two lower levels are occupied in both I_3^- and XeF_2 and one thus obtains a net stabilizing interaction.

How does this picture of three-center electron-rich bonding carry over to our four-coordinate Te in Te_2Br? Let us first establish this electronic analogy in some detail, focusing on $TeBr_4^{2-}$, and then we will look at the local environment of Te1 in Te_2Br.

$TeBr_4^{2-}$ (**7**) is a "classically hypervalent" square planar ion with 2.75 Å Te–Br bonds[25].

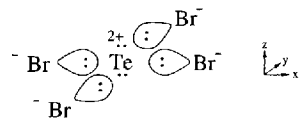

7

Figure 4. An "interaction diagram" for the formation of $[Te_4Br_2]$ from its $[Te_4]^{2+}$ and $[Br_2]^{2-}$ sublattices

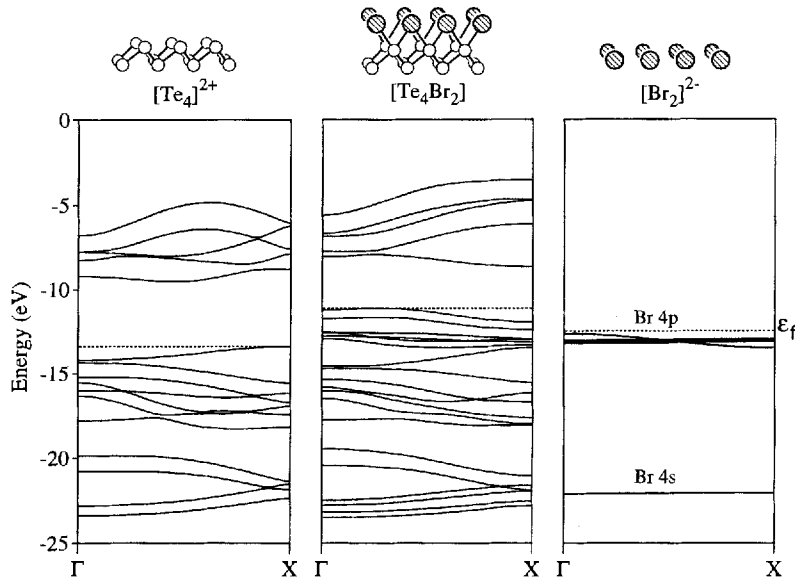

Figure 5. The total DOS (and Br projected DOS, shaded area) and Te1–Br1 COOP curve for $[Te_4Br_2]$; the dashed line in the right-hand plot is the integrated COOP, or average OP, curve

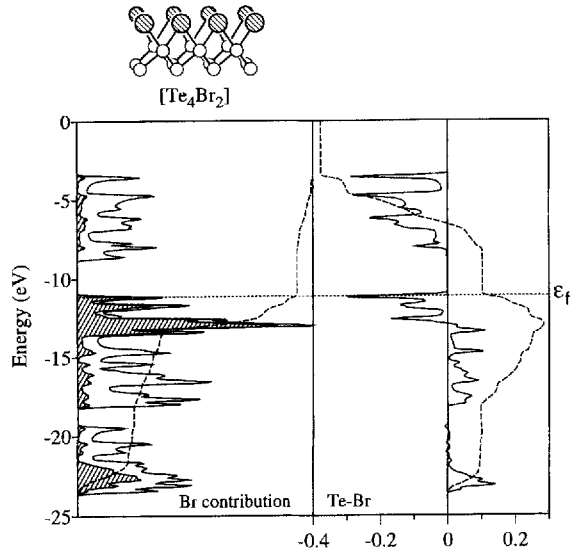

These hypervalent bonds are significantly longer than the 2.51 Å Te–Br single bonds in $TeBr_2$[31,32]. The Te–Br bond lengths in Te_2Br are, as we noted, longer still: 2.90 and 3.02 Å respectively.

An energy level diagram for $TeBr_4^{2-}$ with the Te–Br Molecular Orbital Overlap Population (MOOP) curve (MOOP curves are the molecular equivalent of COOP curves: showing the bonding characteristics of each molecular orbitals) is shown in Figure 6. The levels that have some Te–Br bonding (or antibonding) character are labeled according to their D_{4h} symmetry.

Figure 6. Energy levels (left) and Te–Br MOOP curve (right) for $TeBr_4^{2-}$; the dashed line in the MOOP plot shows the integration of the MOOP curve; symmetry labels are appropriate for the D_{4h} symmetry of $TeBr_4^{2-}$; the shaded block labelled "Br 5p" indicates the location of the linear combinations of Br 5p orbitals which do not interact significantly with the central Te atom

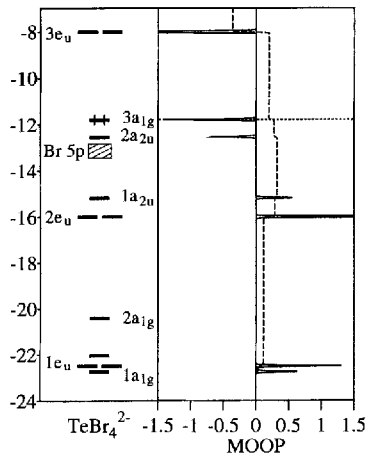

To facilitate eventual comparison with the results for Te_2Br, these calculations for $TeBr_4^{2-}$ were carried out using a Te–Br bond length of 2.90 Å (the Te1–Br1 distance in Te_2Br). Lengthening the Te–Br bonds allows us to directly compare calculated Te–Br overlap populations, but does not qualitatively affect the nature of the orbitals of $TeBr_4^{2-}$. We calculated a Te–Br overlap population (the integration of the MOOP curve up to the HOMO) for $TeBr_4^{2-}$ of 0.19.

We need to analyze the multicenter electron-rich bonding in further detail. The square planar symmetry of $TeBr_4^{2-}$ gives not only a clean $\sigma-\pi$ separation, but also allows us to distinguish between molecular orbitals containing Te 5s (a_{1g}) or $5p_{x,y}$ (e_u) contributions. We will take advantage of this simplification by focusing our attention first on the Te 5s contributions to σ bonding, then we will look at the contributions from the e_u orbitals on Te. Figure 7 shows an interaction diagram for the Te 5s orbital and the 4 Br^- ions in $TeBr_4^{2-}$.

Figure 7. Interaction diagram for the a_{1g} orbitals of $TeBr_4^{2-}$

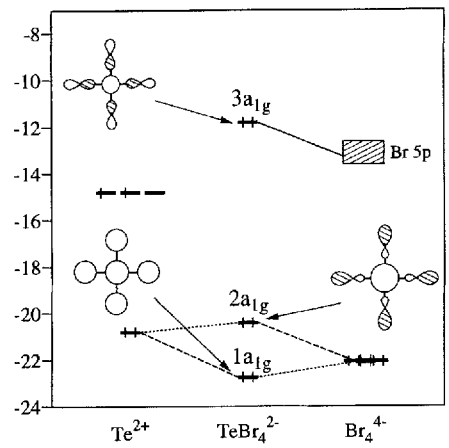

These orbitals follow the usual pattern for a three orbital interaction: the lowest orbital ($1a_{1g}$), is Te–Br bonding, the middle orbital ($2a_{1g}$) is more or less Te–Br nonbonding (this can be most easily seen in the MOOP curve for the system in Figure 6), and the highest level ($3a_{1g}$) is Te–Br antibonding. Thus the net contribution of the a_{1g} set of orbitals (all occupied) to the Te–Br interaction is antibonding. The antibonding $3a_{1g}$ orbital, which corresponds to the second orbital in the classical three-center bonding scheme shown in **6**, is the HOMO of $TeBr_4^{2-}$. Figure 8 shows the analogous interaction diagram for the e_u orbitals of $TeBr_4^{2-}$.

Once again we have a three-orbital system (we count each doubly degenerate e_u set as a single orbital). However, the nature of the bonding here is different from that in the a_{1g} set or orbitals. Inspection of the Te–Br MOOP curve (Figure 6) shows that the middle $2e_u$ level is significantly more strongly bonding than the $2a_{1g}$. This is due to the better energy match between the Te 5p and Br 4p orbitals than between Te 5s and Br 4p. Recall that interaction strength is inversely proportional to the difference in energy between interacting orbitals[30]. In $TeBr_4^{2-}$ both the $1e_u$ and $2e_u$ are occupied, so the net contribution of this set of orbitals to the Te–Br interaction is bonding. The positive total Te–Br overlap population of 0.19 shows that the bonding contributed by the e_u set is stronger than the antibonding contribution from the a_{1g} orbitals.

Figure 8. Interaction diagram for the e_u orbitals of $TeBr_4^{2-}$; a sketch is shown of one member of each doubly degenerate set

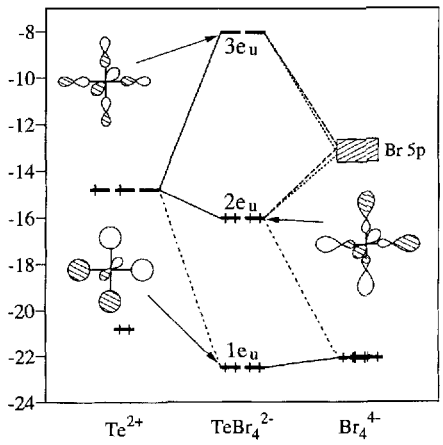

Finally, there are two levels in $TeBr_4^{2-}$ that are of a_{2u} symmetry. These are π bonding and π antibonding between the central Te and the surrounding Br atoms. Since both levels are filled, and since π contributions to bonding are generally weaker than σ contributions, these do not have a strong impact upon the bonding in $TeBr_4^{2-}$. The lower a_{2u} level is more localized on the Te (it is 82% Te in our calculations); this is the p orbital "lone pair" of square-planar hypervalent systems.

Let us first establish more directly the analogy between Te1 in Te_2Br and the hypervalent Te in $TeBr_4^{2-}$. Formally the central Te in $TeBr_4^{2-}$ is Te^{2+} (like formal Xe^{4+} in XeF_4). Suppose we adopt a corresponding formalism at Te1 (or Te4), surrounding it by octet ions Br^- or $Te2^-$ (the Te2–Te3 bond is taken as covalent). Valence structure **8** may make this clearer; then Te1 is formally a Te^{2+}.

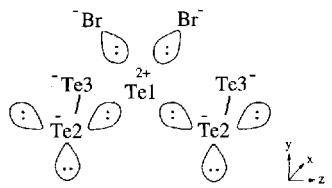

8

The bonding situation changes markedly when we remove the 4-fold rotation symmetry of $TeBr_4^{2-}$ by examining a $Te_3Br_2^{4-}$ molecular model of the Te1 coordination environment in Te_2Br. The Te1–Te2 and Te1–Br1 distances used are the same as those in Te_2Br: 2.84 and 2.90 Å respectively. Before we proceed, a word about the electron count in $Te_3Br_2^{4-}$: we have put a 4– charge on the molecule in order to complete the octet at each atom and keep the electron count the same as it is in $TeBr_4^{2-}$, which is illustrated in the Lewis dot structure shown in **9**. Here the 4 "extra" electrons on the Te2's are indicated with small x's. The electron count at the central Te is consistent with a formal charge of 2+, just as in $TeBr_4^{2-}$.

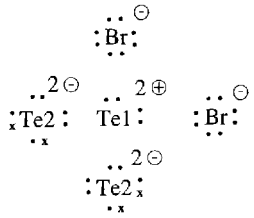

9

The qualitative aspects of the energy level diagram (not shown) for $Te_3Br_2^{4-}$ are similar to those of $TeBr_4^{2-}$, though of course all degeneracies have been removed due to the drop in symmetry from D_{4h} to C_{2v}. The HOMO of $Te_3Br_2^{4-}$ (Figure 9 right) is similar to that of $TeBr_4^{2-}$ (Figure 9 left).

Figure 9. Contour plots of the Highest Occupied Molecular Orbitals (HOMOs) of $TeBr_4^{2-}$ (left) and $Te_3Br_2^{4-}$ (right)

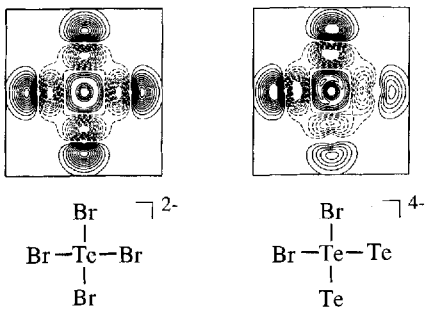

In $TeBr_4^{2-}$, the HOMO consists of Te 5s and Br s–p hybrids and is symmetrically antibonding between the Te and all four Br's. The situation is different in one very important way in $Te_3Br_2^{4-}$: the loss of the 4-fold symmetry allows some Te1 5p character to mix into the HOMO. The effect of this s–p mixing at the central Te1 is to decrease the amount of Te1–Te2 antibonding character in the HOMO while *increasing* the amount of Te1–Br antibonding. The increase in Te1–Br antibonding in this one level significantly weakens the the Te1–Br bonding built up in other orbitals, leaving a net Te1–Br overlap population of 0.10. In the extended structure of Te_2Br, the two Te–Br antibonding bands located just below the Fermi level are derived from the HOMO of our $Te_3Br_2^{4-}$ molecular model. This is the orbital that is responsible for the weakening of the Te–Br bonding (and the resulting long Te–Br bonds) in Te_2Br as well.

In summary, we see multi-center electron-rich bonding in $TeBr_4^{2-}$ and in a $Te_2TeBr_2^{4-}$ model for Te_2Br. It is there, but there are also orbital reasons why the Te–Br bonds in the Te_2Br model are weak, weaker than in $TeBr_4^{2-}$.

$[Te_{15}Br_4]^{2+}$

It is straightforward to build up the $[Te_{15}Br_4]^{2+}$ chains found in $[Te_{15}Br_4][MoOBr_4]_2$ from those found in the experimental structure of Te_2Br[15]. If we take a $[Te_4Br_2]$ chain, **5** and remove the row of Br^- ions closest to the Te4's (the

numbering used is from **2**), we arrive at a $[Te_4Br]^+$ chain, **10**.

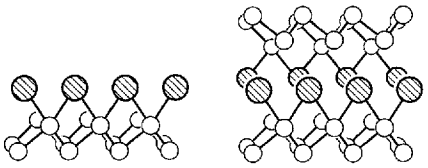

$[Te_4Br]^+$ $[Te_8Br_2]^{2+}$

10 **11**

Pairing two of these chains gives $[Te_8Br_2]^{2+}$, **11**. The remaining step, not shown here, is to double the size of the unit cell along the propagation direction (giving $[Te_{16}Br_4]^{4+}$) and to remove one of the divalent Te4 atoms as Te^{2+}, giving us $[Te_{15}Br_4]^{2+}$.

The rationale for removing a Te from the chain as Te^{2+} is the following: If we consider the divalent Te1 and Te4 atoms to be neutral and the three-coordinate Te2 and Te3 to each carry a 1+ formal charge, then we arrive at the $[Te_4Br]^+$ repeat unit shown in **12** left (the Br^- ions are omitted for clarity).

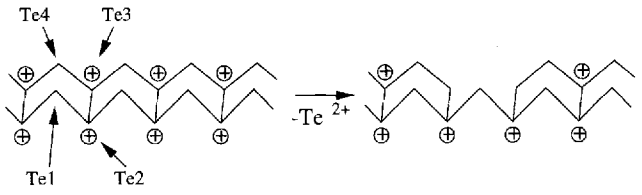

12

These formal charges are consistent with our calculated net charges on the two-coordinate (<+0.07) and three-coordinate (~+0.58) Te atoms. Removing one two-coordinate Te leaves two formerly three-coordinate Te3's with only two bonding contacts (shown on the right in **12**). So these "newly two-coordinate" Te's become formally neutral. This implies that the Te4 has to be removed as Te^{2+}. The calculated net charges on the Te3 atoms adjacent to the defect site (~−0.11) are again consistent with this view[33].

The same formal charges can be arrived at by considering a Lewis structure of the coordination environment about Te3 (**13**).

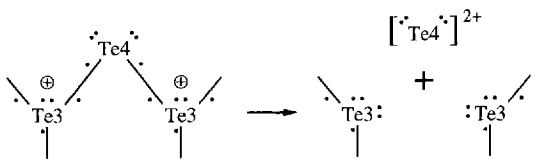

13

If we want the octet about Te3 to remain complete when a Te4 is removed, the Te3−Te4 bond must be cleaved heterolytically, leaving us with two neutral Te3's and a $Te4^{2+}$.

Figure 10 shows the development of the electronic structure of the $[Te_{15}Br_4]^{2+}$ chains of $[Te_{15}Br_4][MoOBr_4]_2$ as we build the chains from those found in the Te subhalide Te_2Br.

When a row of Br^- ions is removed to give $[Te_4Br]^+$, some of the bands disappear (particularly apparent is the loss of one of the Te−Br antibonding bands just under ε_f). Otherwise there is little perturbation of the band structure. When two $[Te_4Br]^+$ chains are paired to give $[Te_8Br_2]^{2+}$ the bands are doubled in number. There are once again two Te−Br antibonding bands underneath ε_f. Again the band structure is rather similar to that of $[Te_4Br_2]$. Doubling the unit cell along the propagation direction and removing a Te^{2+} to give $[Te_{15}Br_4]^{2+}$ results in a band structure (not shown) which is quite similar to that of $[Te_8Br_2]^{2+}$.

The $[MoOBr_4]^-$ Chain

We now move on to the $[MoOBr_4]^-$ chains of $[Te_{15}Br_4][MoOBr_4]_2$, which are made up of distorted vertex-sharing octahedra running in one dimension. The Mo atoms are each surrounded by four equatorial Br atoms (Mo−Br distances are 2.49 and 2.52 Å in $[MoOBr_4]^-$) and have one close (1.62 Å) oxygen neighbor. The other axial Mo−O contact (which completes the octahedron) is significantly longer: 2.41 Å. Each axial O is shared between two octahedra to form the chain. The structure is shown schematically in **1** above. If the equatorial Mo−Br contacts were all the same length the site symmetry of the Mo atoms would be C_{4v}. Since the experimental structure shows a slight Mo−Br_{eq} distortion, we will refer to the geometry as "pseudo-C_{4v}".

The calculated band structure of a $[MoOBr_4]^-$ chain excised from the full $[Te_{15}Br_4][MoOBr_4]_2$ structure, shown in Figure 11, is very similar to that of $[MoNCl_4]^-$, which has already been carefully analyzed[34]. In these systems the observed distortions from ideal octahedral symmetry are primarily due to mixing between high lying occupied M−O π and low lying unoccupied M−O π* orbitals (essentially a second order Jahn-Teller effect).

The primary difference between the band structures of $[MoNCl_4]^-$ and $[MoOBr_4]^-$ is the position of the Fermi level. In $[MoNCl_4]^-$ the Mo is formally 6+ and therefore has no 4d electrons. However, in $[MoOBr_4]^-$ the Mo atoms are in the 5+ oxidation state, i.e. they have a single 4d electron remaining. This single electron in the very flat (bandwidth <0.1 eV) b_2 band is likely to be responsible for the observed paramagnetism of $[Te_{15}Br_4][MoOBr_4]_2$.

The b_2 orbital (sketched in Figure 11) is π antibonding between the Mo and Br atoms and has δ symmetry between unit cells. The δ overlap between two Mo atoms at 4.036 Å (the lattice spacing in $[Te_{15}Br_4][MoOBr_4]_2$) is extremely small: 0.0008. As there is (by symmetry) no oxygen contribution to this orbital, its band width is determined by this small overlap matrix element and thus the band is nearly flat.

Combining the Sublattices and a Reason for the Defect Structure

When we combine the $[Te_{15}Br_4]^{2+}$ and $[MoOBr_4]^-$ subchains to form the full three-dimensional structure of

Figure 10. The band structures in the vicinity of ε_f of: (a) $[Te_4Br_2]$ (i.e. Te_2Br), (b) $[Te_4Br]^+$, and (c) $[Te_8Br_2]^{2+}$

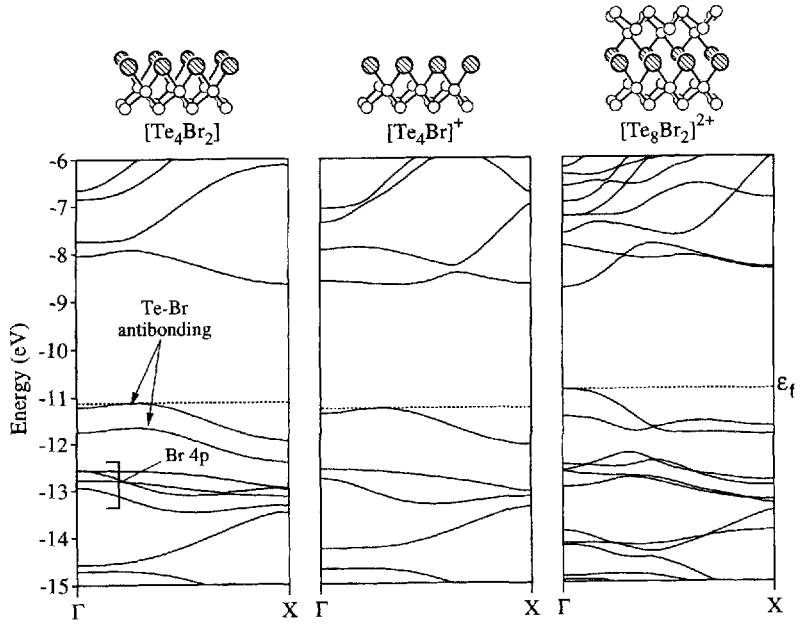

Figure 11. The band structure of $[MoOBr_4]^-$ in the region of the Fermi level; the symmetry labels given are those appropriate for the pseudo-C_{4v} coordination environment of the Mo atoms; sketches of the b_2 orbital at Γ and X are shown at either side of the band structure

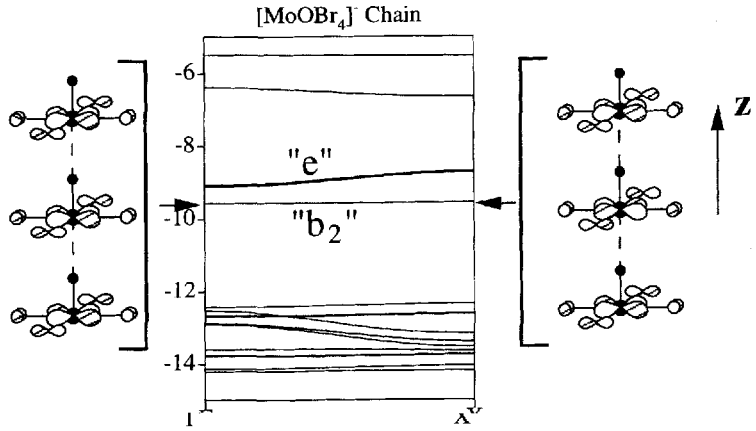

$[Te_{15}Br_4][MoOBr_4]_2$, the chains do not interact significantly with each other. The changes in electronic structure are really very small. This can be seen clearly by comparing the DOS's of $[Te_{15}Br_4][MoOBr_4]_2$ and the result of summing the calculated DOS's of the two sublattices ($[Te_{15}Br_4]^{2+}$ and $[MoOBr_4]^-$), Figure 12.

There are only small differences between the calculated DOS's of $[Te_{15}Br_4][MoOBr_4]_2$ and the summed sublattices, particularly in the vicinity of ε_f. $[Te_{15}Br_4][MoOBr_4]_2$ is thus effectively composed of one-dimensional subchains that interact only electrostatically. This conclusion is supported by a comparison of calculated net charges and average COOP values (not shown), which show insignificant changes on moving from the sublattices to the full structure. This lack of perturbation arises because there is little orbital overlap between chains. There is also little charge transfer between sublattices because the Highest Occupied and Lowest Unoccupied Crystal Orbitals (HOCOs and LUCOs) of the $[MoOBr_4]^-$ chains come in the gap between the HOCO and LUCO of the $[Te_{15}Br_4]^{2+}$ chains.

The nature of the charge transfer enables us to make a very simple argument for the experimentally observed presence and number of Te vacancies in the $[Te_{15}X_4]_n[MOX_4]_{2n}$ structure type. Suppose we were to form $[Te_{16}Br_4][MoOBr_4]_2$ by putting *back* the Te^{2+} we removed in our *aufbau* approach to $[Te_{15}Br_4]^{2+}$. Now each Te subchain would have a formal charge of 4+. This requires the Mo chains to each have a 2− charge, placing an additional electron in the b_2 band. The pairing energy associated with filling this very localized crystal orbital would be very destabilizing[35]. If we were to remove another Te^{2+} from the Te subchains, giving $[Te_{14}Br_4]^0$ and $[MoOBr_4]^0$, then the favorable electrostatic interactions between the Te and Mo subchains would be gone. There would be nothing holding the crystal together[36].

Figure 12. A comparison of the DOS of $[Te_{15}Br_4][MoOBr_4]_2$ (solid line) and the sum of the DOS's of $[Te_{15}Br_4]^{2+}$ and $[MoOBr_4]^-$ (dashed line); the right panel shows a zoomed view of the region around ε_f; these curves also carry integrations of the DOS, which emphasize the similarities; the DOS units are states/eV

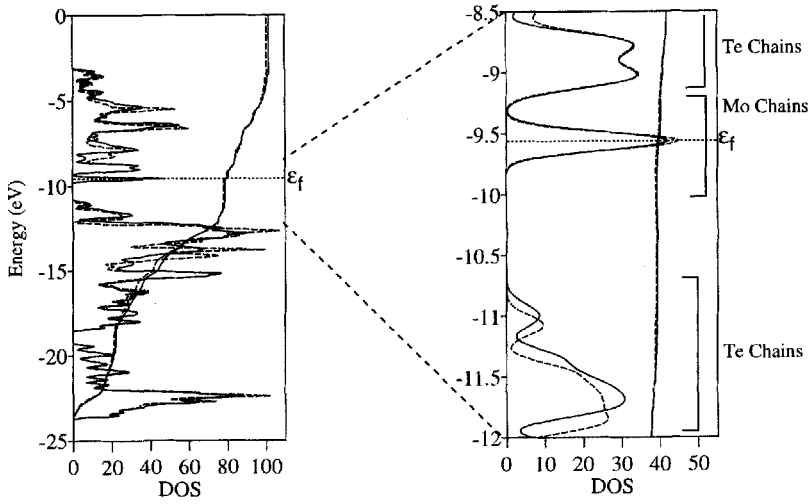

The observed defect stoichiometry of $[Te_{15}Br_4][MoOBr_4]_2$ is thus the result of a fine balance between a destabilizing electron pairing in the HOCO of the Mo subchains were the defects removed and dimunition of the Madelung forces which hold the chains together upon addition of defects.

Conclusions

$[Te_{15}Br_4][MoOBr_4]_2$ is a primarily one-dimensional material made up of $[Te_{15}Br_4]^{2+}$ and $[MoOBr_4]^-$ subchains held together by electrostatic (as opposed to orbital) interactions. The electronic structure of the $[Te_{15}Br_4]^{2+}$ subchains is very similar to that of the Te subhalide Te_2Br. There are strong signs of hypervalency at the "square planar" Te sites in both $[Te_{15}Br_4]^{2+}$ and Te_2Br. The experimentally observed paramagnetism in $[Te_{15}Br_4][MoOBr_4]_2$ arises from an unpaired electron in the b_2 band of the $[MoOBr_4]^-$ chain. While within the extended Hückel model it is not possible to predict the origin of the semi-conducting properties of the material, it seems reasonable to assume that these arise due to the $[Te_{15}Br_4]^{2+}$ subchains.

We are grateful to the *National Science Foundation* for its support of our work through Research Grant CHE 94-08455. Norman Goldberg thanks the *Deutsche Forschungsgemeinschaft* for a fellowship that made his stay at Cornell possible. We would also like to thank *Silicon Graphics* for their generous donation of the computer hardware that was used in this work.

Experimental Section

Computational Details: All calculations were performed using the program YAeHMOP, developed by one of the authors (G.L.)[37]. The parameters used in the calculations are given in Table 1. All parameters were taken from a standard set[38].

Table 1. Parameters used in the extended Hückel calculations

Atom	Orbital	H_{ii}(eV)	ζ_1	ζ_2	C_1	C_2
Mo	4d	-10.50	4.540	1.900	0.6097	0.6097
	5s	-8.34	1.96			
	5p	-5.24	1.90			
Te	5s	-20.80	2.750			
	5p	-14.80	2.160			
Br	4s	-22.07	2.588			
	4p	-12.10	2.131			
O	2s	-32.30	2.275			
	2p	-14.80	2.275			

[1] P. Böttcher, *Angew. Chem. Int. Ed. Engl.* **1988**, *27*, 759.
[2] M. A. Ansari, J. M. McConnache, J. A. Ibers, *Acc. Chem. Res.* **1993**, *26*, 574.
[3] W. Sheldrick, M. Wachold, *Chem. Commun.* **1996**, 607.
[4] W. Sheldrick, M. Wachold, *Angew. Chem. Int. Ed. Engl.* **1995**, *34*, 450.
[5] Q. Liu, N. Goldberg, R. Hoffmann, *Chem. Eur. J.* **1996**, *2*, 390.
[6] X. Zhang, J. Li, B. Foran, S. Lee, H.-y. Guo, H. T., C. Kannewurf, M. Kanatzidis, *J. Am. Chem. Soc.* **1995**, *117*, 10513.
[7] J. Beck, G. Bock, *Angew. Chem. Int. Ed. Engl.* **1995**, *34*, 2559.
[8] J. Beck, *Chem. Ber.* **1995**, *128*, 23.
[9] J. Beck, K.-J. Schlitt, *Chem. Ber.* **1995**, *128*, 763.
[10] J. Beck, G. Bock, *Z. anorg. allg. Chem.* **1994**, *620*, 1971.
[11] T. Chivers, *J. Chem. Soc. Dalton Trans.* **1996**, 1185.
[12] J. Beck, *Angew. Chem. Int. Ed. Engl.* **1994**, *33*, 163.
[13] M. Kanatzidis, *Angew. Chem. Int. Ed. Engl.* **1995**, *34*, 2109.
[14] J. A. Beck, M. A. Pell, J. Richter, J. A. Ibers, *Z. anorg. allg. Chem.* **1996**, *622*, 473.
[15] V. R. Kniep, D. Mootz, A. Rabenau, *Z. anorg. allg. Chem.* **1976**, *422*, 17.
[16] The electronic structure, properties, and distortions of this type of chain have previously been analyzed in great detail in Reference 34, so we will not dwell on them here.
[17] There are also small differences in bond lengths between $[Te_{15}X_4]^{2+}$ and Te_2X.[14,15] For example, the Te-Te and Te-Br

distances for X = Br are (in Ångströms): Te1−Te2 = 2.84 (2.85), Te2−Te3 = 2.92 (2.85), Te3−Te4 = 2.81 (2.74), Te1−Br1 = 2.90 (3.00), Te4−Br = 3.02 (3.29). Distances for $[Te_{15}Br_4]^{2+}$ are in parentheses. The Te−Br distances are significantly longer in $[Te_{15}Br_4]^{2+}$, however as will become clear later, this does not have a large impact on the electronic structure since the Te−Br interactions are primarily electrostatic.

[18] R. Hoffmann, *Solids and Surfaces: A Chemist's View of Bonding in Extended Structures*; VCH, Weinheim, **1988**.

[19] R. Hoffmann, *J. Chem. Phys.* **1963**, *39*, 1397.

[20] R. Hoffmann, *J. Chem. Phys.* **1964**, *40*, 2745.

[21] R. Hoffmann, *J. Chem. Phys.* **1964**, *40*, 2474.

[22] T. Hughbanks, R. Hoffmann, *J. Am. Chem. Soc.* **1983**, *105*, 3528.

[23] The results shown here are for the Te2−Te1 chain of Te_2Br. The Te3−Te4 chain, which has a slightly shorter (0.03 Å) Te−Te bond, has a similar electronic structure.

[24] R. Hoffmann, C. Janiak, C. Kollmar, *Macromolecules* **1991**, *24*, 3725.

[25] S. Pohl, W. Saak, B. Krebs, *Z. Naturforsch.* **1985**, *40b*, 251.

[26] R. Rundle, *J. Am. Chem. Soc.* **1963**, *85*, 112.

[27] R. Rundle, *J. Am. Chem. Soc.* **1979**, *101*, 5057.

[28] G. Pimentel, *J. Chem. Phys.* **1951**, *16*, 446.

[29] R. Gillespie, *Molecular Geometry*; Van Nostrand-Rheinhold, London, **1972**.

[30] T. Albright, J. Burdett, M.-H. Whangbo, *Orbital Interactions in Chemistry*; John Wiley, New York, **1985**.

[31] W. Grethers, *Ann. Physik* **1936**, *26*, 1.

[32] M. Rogers, R. Spurr, *J. Am. Chem. Soc.* **1947**, *69*, 2102.

[33] The X-ray structure of $[Te_{15}Br_4][MoOBr_4]_2$ does not distinguish unambiguously between a random or ordered arrangement of the vacant Te4 sites. To be able to perform the tight-binding calculations, an ordered arrangement was needed. The unit cell used in our calculations on $[Te_{15}Br_4][MoOBr_4]_2$ was quadrupled along the b direction in order to be able to accommodate one missing Te4 in each of the 4 $[Te_{15}Br_4]^{2+}$ chains in the cell, i.e. the unit cell used had the stoichiometry: $[Te_{15}Br_4]_4[MoOBr_4]_8$.

[34] R. A. Wheeler, M.-H. Whangbo, T. Hughbanks, R. Hoffmann, J. K. Burdett, T. A. Albright, *J. Am. Chem. Soc.* **1986**, *108*, 2222.

[35] While it is impossible to calculate this pairing energy within a one-electron theory such as the extended Hückel method, past work by other groups on transition metal systems leads us to believe that the destabilization associated with filling the b_2 band of $[MoOBr_4]^-$ would be quite large indeed (> 1 eV).[39]

[36] We could also think about compensating the 4+ charge on the Te sublattices by doubling the number of $[MoOBr_4]^-$ chains in the crystal, thus changing the stoichiometry to $[Te_{16}Br_4][MoOBr_4]_4$. However, going back and looking at the packing of the subchains in the observed stoichiometry, it is very difficult to imagine a packing with twice as many $[MoOBr_4]^-$ units that would not have a large number of electrostatically unfavorable like-charge−like-charge contacts.

[37] G. A. Landrum, Yet Another extended Hückel Molecular Orbital Package (YAeHMOP) is available on the World Wide Web at: http://overlap.chem.cornell.edu:8080/yaehmop.html, **1995**.

[38] S. Alvarez, unpublished results, **1993**.

[39] P. Anderson, *Phys. Rev.* **1959**, *115*, 2.

[96227]